Superconductor Science and Technology

Comparing the performance of 850 GHz integrated bias-tee superconductor-insulator-superconductor (SIS) mixers with single- and parallel-junction tuner

To cite this article: B-K Tan *et al* 2022 *Supercond. Sci. Technol.* **35** 125008

OPEN ACCESS
IOP Publishing
Superconductor Science and Technology
Supercond. Sci. Technol. **35** (2022) 125008 (11pp)
https://doi.org/10.1088/1361-6668/ac9d6e

Comparing the performance of 850 GHz integrated bias-tee superconductor-insulator-superconductor (SIS) mixers with single- and parallel-junction tuner

B-K Tan[1,*], K Rudakov[2], V P Koshelets[3], A Khudchenko[4], A M Baryshev[2] and G Yassin[1]

[1] Department of Physics (Astrophysics), University of Oxford, DWB Keble Road, OX1 3RH Oxford, United Kingdom
[2] Kapteyn Astronomical Institute, Groningen 9747 AD, The Netherlands
[3] Kotel'nikov Institute of Radio Engineering and Electronics, Russian Academy of Science, Moscow 125009, Russia
[4] Astro Space Center of Lebedev Physical Institute, Russian Academy of Science, Moscow 117997, Russia

E-mail: boonkok.tan@physics.ox.ac.uk

Received 30 June 2022, revised 12 October 2022
Accepted for publication 25 October 2022
Published 7 November 2022

Abstract

We present and compare the design and performance of two 850 GHz radial probe fed superconductor-insulator-superconductor mixers, where the antenna is aligned perpendicular to the E-Plane of the input full-height rectangular waveguide connected to a multiple flare-angles smooth-walled horn. Both designs are comprised of 0.5 μm^2 hybrid niobium/aluminium-nitride/niobium-nitride tunnel junction, fabricated on top of a niobium titanium nitride ground plane with an Al wiring layer. The entire superconducting circuit is supported with a 40 μm thick quartz substrate. The major difference between the two designs is the method used to cancel out the parasitic junction capacitance for broadband performance. The first design utilises two identical junctions connected in parallel with a short transmission line to convert the capacitance of one junction into the equivalent inductance of the other junction, commonly known as the twin-junction tuning scheme; whilst the second design employs an end-loaded scheme with only one tunnel junction. We found that both methods offer similar radio frequency performances, with close to 2$\times$ the double sideband quantum noise temperature, but the twin-junction design is more resilient to fabrication tolerances. However, the end-loaded design offers a much better intermediate frequency (IF) bandwidth performance, made possible by the sub-micron and high current density tunnel junction technology. The improved IF performance is important for many millimetre (mm) and sub-mm observatories, such as future upgrades of Atacama Large Millimetre/sub-mm Array receivers, as well as forthcoming space-borne far-infrared missions. Therefore, we conclude that the single-junction mixer design is the preferred option for THz applications, as long as the fabrication error can be minimised within a certain limit.

* Author to whom any correspondence should be addressed.

Keywords: broadband terahertz technology, superconductor-insulator-superconductor (SIS) mixer, twin-junction, end-loaded tuner, millimetre/sub-millimetre astronomy, radial probe

(Some figures may appear in colour only in the online journal)

1. Introduction

Spectroscopic observations near and above the 1.0 THz window are scant even at dry sites, such as the Chajnantor plateau, due to the scarcity of the premium weather conditions needed. However, these THz frequency windows contain a host of crucial spectral lines that would allow astronomers to study the dense core of giant molecular clouds where star formation took place and probe galaxy evolution processes in the early Universe via the highly redshifted lines [1–4]. Therefore, it is important to maximise the sensitivity of the heterodyne receivers to fully take advantage of the good weather condition when available. However, the radio frequency (RF) and intermediate frequency (IF) performance of THz superconductor-insulator-superconductor (SIS) mixers such as the high-frequency band array (790–950 GHz) of the Carbon Heterodyne Array of the Max-Planck Institute Plus [5–8] still yet to achieve the same quantum-limited sensitivity compared to the lower frequency band mixers. Nevertheless, recent advances in modern planar superconducting circuit and tunnel junction fabrication techniques have made possible further improvement of the mixer performance by utilising (a) sub-micron high current density high-gap tunnel junction, (b) full-height waveguide feed antenna for ease of fabrication and (c) innovative tuning methodologies to achieve broad RF and IF coverage with quantum-limited sensitivity.

In this paper, we report on two THz SIS mixers fabricated using sub-micron hybrid niobium/aluminium-nitride/niobium-nitride (Nb/AlN/NbN) tunnel junction(s) to mitigate the limitations imposed by the commonly-used full-niobium technology. At THz frequencies, the bandwidth requirement of the feed antenna becomes considerably less vital as the percentage bandwidth of the atmospheric window becomes relatively narrower, but the junction tuning becomes more crucial as the ωRC product increased substantially, affecting both the RF and IF noise-bandwidth performance. Therefore, we have developed two mixer designs comprising two different junction tuning methods i.e. the twin-junction tuning and the end-loaded tuner with a single tunnel junction, to compare their performances. Furthermore, as the dimension of most, if not all, of the THz mixer circuit components becomes comparatively smaller, we also investigate how the fabrication tolerance of various critical dimensions of the mixer circuit may affect the performance of these two designs.

1.1. Junction and planar circuit technology considerations

In principle, an all-Nb tunnel junction can operate up to twice its gap frequency ($f_{\rm gap} \approx 680$ GHz) [9–11], but the mixer operation becomes less ideal and the performance starts to deteriorate rapidly at a higher frequency. Furthermore, approaching frequency close to $2 \times f_{\rm gap}$, a large portion of the photon step would be suppressed, hence limiting the range where an optimal biasing point can be located. Therefore, there have been extensive efforts in recent years to search for higher gap superconductors, such as NbN or niobium titanium nitride (NbTiN) as replacements, as well as exploring new insulating materials to achieve higher current density to relax the ωRC requirement. Table 1 shows some of the recent examples of THz SIS mixer development focused around Atacama Large Millimetre/sub-millimetre Array (ALMA) Band-10 and 11 range. As can be seen, the deployment of high-gap tunnel junctions, such as all-NbN or all-NbTiN junctions remains elusive because of the difficulty in fabricating a high-quality barrier between the electrodes. Therefore, most efforts have been diverted to the use of hybrid junction, for which standard Nb film is used as the bottom electrode to circumvent the thin insulating barrier issue, while a higher gap superconductor is deposited as the top electrode [7, 12] to increase the gap voltage to $\sim$3.5 mV, high enough to give a quantum-limited performance at supra-THz frequencies.

Apart from the material used to form the tunnel junction, the choice of conductive layers used for realising the mixer circuit is another important consideration when designing a THz mixer. Nb becomes lossy above $f_{\rm gap}$ hence ideally should be replaced with a higher gap superconductor. However, as reported frequently in the literature, embedding tunnel junctions between non-Nb superconductors proved to be challenging, especially when a high gap superconductor is deposited on top of the tunnel junction. For example, Khudchenko *et al* [7] showed that the lossy NbN film degrades the tunnel junction quality substantially, lowering the gap voltage from the supposed 3.6 mV to about 3.1 mV, hence affecting the mixer performance. Therefore, most of the examples shown in table 1 replaced only the bottom ground layer with a high gap superconductor, while using either Nb or a normal metal for the top layer.

2. THz mixer designs and electromagnetic simulations

Different from most examples shown in table 1 which utilise a bowtie probe as input antenna, we employ a radial probe antenna commonly used in lower frequency bands. We have shown in previous works [7, 14, 15] that these probe mixers mounted perpendicular to the E-plane of a half-height rectangular waveguide can produce noise performances exceeding that of current ALMA Band-10 mixers. However, due to the difficulties in machining a high aspect ratio input waveguide, especially the backshort, we now opt for a full-height

Table 1. Thin films and tunnel junction technologies utilised in various THz SIS mixers reported in the literature. The table is by no mean complete but shows a range of various approaches explored to achieve a quantum-limited performance near and above the ALMA Band-10 range.

Reference		Yassin *et al* [13][a]	Karpov *et al* [12][b]	Uzawa *et al* [11]	Kojima *et al* [10][c]	Jackson *et al* [9][d]	This work
Wiring Layer		Normal Metal	Gold	NbTiN	NbTiN	Al	Al
Dielectric Layer		—	—	SiO_2	SiO_2	SiO_2	SiO_2
Ground Layer		Normal Metal	Epitaxial Nb	NbTiN	Al	NbTiN	NbTiN
Tunnel Junc.	Top	NbN	NbTiN	Nb	Nb	Nb	NbN
	Insulator	AlN	AlN	AlN	AlO_x	AlO_x	AlN
	Bottom	Nb	Nb	Nb	Nb	Nb	Nb
V_{gap} (mV)		3.5	3.5	2.8	2.7	2.8	3.15
J_c (kA cm^{-2})		25	30	15	10	6.5–13	30
Junc. Area (μm^2)		0.3–0.6	0.25	1	0.785	1	0.5
RF range (THz)		—	1.1–1.26	0.78–0.95	0.75–1.0	0.8–0.96	0.78–0.95
IF range (GHz)		—	4–8	—	4–12	4–8	—
DSB Noise (K)		—	350–450	—	100–200	220–340	—
Antenna		—	Twin slot	Bowtie	Bowtie	Bowtie	Rad. probe
Waveguide		—	Lens	Full	Full	Half	Full
Tuner		—	Twin-junc.	Twin-junc.	Twin-junc.	Twin-junc.	1 & 2 junc.

[a] The report highlighted some fabrication issues when embedding the junction between NbTiN layers, and suggested a thin gold interface layer between the NbTiN and the junction electrode. The authors only reported on the tunnel junction characterisations without full mixer operation.
[b] Reported similar issues and potential solution as above.
[c] Note that the mixer design reported here comprising inverted microstrip structure, hence the tunnel junction is actually fabricated on top of the NbTiN layer instead of Al.
[d] The authors noted that the drop in mixer sensitivity is caused by the smaller penetration depth in the NbTiN film.

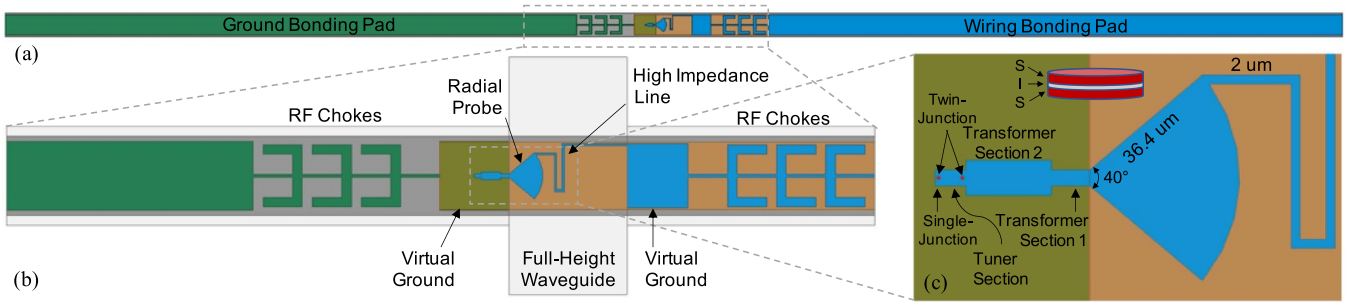

Figure 1. (a) Layout of the THz mixer chip with the superconducting planar circuits fabricated on top of a 1.62 mm long, 80 μm wide, and 40 μm thick quartz substrate. (b) Zoomed-in of the mixer chip showing the radial probe antenna, tunnel junction tuner circuit, virtual grounds, high impedance line and the RF chokes. (c) Detail of the radial probe and the twin-junction tuner circuit. In the case of single-junction tuning, the first (right-hand-side) junction is removed.

waveguide design. This is important for future upgrades such as sideband separating and array operation, as the machining tolerance of the waveguide could affect the balanced performance of the overall receiver.

Figure 1 shows the layout of our new mixer designs. The radial probe is positioned along the E-plane axis of a 120 × 240 μm backshort, where the probe is extended to about 35% of the full waveguide height to achieve maximum coupling. A high impedance line is used to connect the radial probe to the virtual ground pad at the other end of the chip to form the integrated bias-tee setup [16] for IF connections and DC biasing. The 'vertical' sections of high impedance strips perpendicular to the E-field lines are presented as an open-circuited element to the incoming fields, hence avoiding a short-circuited path, which would otherwise significantly reduce the coupling to the probe. Two large pads on either side of the chip are used to provide a 'virtual ground' effect such that they present a 'closed' path for the incoming waves from the input waveguide to continue propagation via capacitive coupling to the waveguide walls, and hence prevent the energy leakage into the slot where the chip is mounted. Finally, three-section high-low impedance RF chokes are employed at both ends of the chip to block the propagation of the RF signal towards the IF path. The entire structure including the backshort, but without the tuning circuit, is then optimised using Ansys high frequency structure simulator (HFSS), taking into account the effect of complex surface impedance, dielectric material and other factors [17] that cannot be accurately calculated from standard transmission line theory, for maximum coupling to the probe antenna across the desired bandwidth.

The mixer circuit comprising one or two 0.5 μm^2 high current density (30 kA cm^{-2}) SIS tunnel junctions, depending on

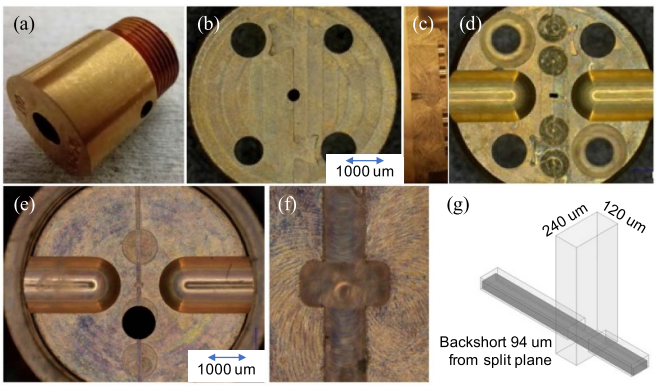

Figure 2. (a) The drilled smooth-walled horns with a circular waveguide output. (b) The front side, (c) cross-section and (d) the rear side view of the direct machined split transition disk, showing the rectangular-to-circular waveguide transition. (e) Top view of the direct machined back-piece hosting the THz mixer chip. (f) Zoomed-in image of the backshort and channel of the back-piece where the mixer chip will be aligned and mounted. (g) Sketch illustrating how the mixer chip would be mounted on the back-piece, with the substrate aligned within the milled channel. The channel width is 100 μm with a depth of 60 μm.

the tuner scheme used to tune out the parasitic junction capacitances, either a twin-junction or an end-loaded method. The top and bottom electrodes of the Nb/AlN/NbN tunnel junctions are both 100 nm thick, with the junction normal resistance of 10 Ω μm^2 and junction capacitance of 90 fF μm^{-2}. The junctions are fabricated on top of a 300 nm thick NbTiN ($T_c = 14.1$ K, resistivity $R = 85$ $\mu\Omega$ cm) ground plane, with a 250 nm Silicon Dioxide (SiO_2) dielectric layer and a 500 nm thick Al ($T_c = 1.2$ K, $R = 0.56$ $\mu\Omega$ cm) layer overlaid on top to form the microstrip transmission line. The entire superconducting circuit is supported by a 40 μm thick quartz substrate, mounted along a long channel on the back-piece where the normal vector of the chip points towards the direction of the propagation of the incoming wave, as shown in figure 2.

The back-piece is aligned to the circular waveguide output of the feed horn via a circular-to-rectangular transition disk, fabricated using split block technology. In contrast to most THz mixers, we use an easy-to-fabricate smooth-walled horn instead of a corrugated horn, to pave way for the possibility of constructing a large focal plane THz array for deployment in future astronomical projects such as the Origin Space Telescope [18], the Far-InfraRed Spectroscopic Surveyor [19], Fred Young Sub-millimetre Telescope (formerly known as Cerro Chajnantor Atacama Telescope-Prime) [20] and the Millimetron Space Observatory [21]. The whole assembly (feed horn, transition and back-piece) is then slotted into an ALMA Band-9 styled mixer block [22] modified for operation between 787–950 GHz.

2.1. Twin-junction versus end-loaded tuning scheme

As shown in table 1, all of the examples listed make use of the popular twin-junction scheme [23–25] to tune out the parasitic capacitance at wide RF frequency range. In principle, using one or two junctions of the same size should only have a small effect on the RF performance. This is because with two junctions connected in parallel, the normal resistance is halved but the total capacitance becomes twice higher, hence the ωRC product remains the same. However, the same is not true for the IF behaviour. In our case, the output of the mixer chip is connected directly to the 50 Ω environment without any intermediate impedance transformer stage. Therefore, ideally, it is preferable to have the output impedance of the mixer closer to 50 Ω. Hence, the lower normal resistance of the twin-junction design becomes a disadvantage here. More importantly, the IF capacitance is doubled with two junctions in parallel, which may affect the IF bandwidth as the resonance cutoff at the microwave frequency range is now nearer to the IF band [26].

Therefore, to investigate the pros and cons of single and double-junction tuning schemes, we further explore an alternative solution by using only a single tunnel junction with the end-loaded tuning method. It is possible to utilise the end-stub design [27] as well, but since both single-junction tuners would behave similarly for our analysis here, we focused only on the end-loaded scheme that has a closer resemblance to the twin-junction design topologically. We should emphasise that to compare the two solutions directly without unnecessarily complicating the mixer design with too many changes, only the tuning circuit part shown in figure 1(c) is different here, while the design of the rest of the mixer such as a radial probe, high impedance line, RF chokes etc remains the same.

Figure 1 (c) shows in detail the tuning sections of our mixer chip. For both designs, a short microstrip section (herein after transformer section 1 abbreviated as TX_1) is connected to the output of the probe to provide a bridging impedance sector. Another low impedance section (TX_2) is then used to connect TX_1 with the tuner section where the junction(s) are embedded. The characteristic impedance (Z_0) of the tuner section is chosen to be close to the normal resistance of the junction(s). The only difference between the two designs is that the first junction located between TX_2 and the tuner section is removed for the end-loaded scheme. For both cases, the entire tuning circuit is then optimised using HFSS to achieve maximum coupling to the junction(s) over the broadest possible bandwidth, without any changes to the remaining mixer circuits.

The final optimised dimensions of the tuner components are tabulated in table 2, and the scattering matrix responses of both complete mixers are presented in figure 3. As can be seen, we managed to cover the entire ALMA Band-10 frequency range for both cases, but the twin-junction device shows a slightly better and wider junction coupling performance. However, one rather striking and surprising outcome from the optimisation process is that one noted immediately that in figure 3(a), the power coupling from the input waveguide to the second junction located near the end of the tuner section ($S_{4,1}$) is much higher than the first junction ($S_{3,1}$). This implies that the contribution of the first junction towards the overall performance is mainly towards the higher part of the band, complementing that of the second junction, hence resulting in broader bandwidth performance compared to the end-loaded design.

Table 2. Dimensions of the various sections forming the twin-junction and the end-loaded tuning circuit.

		TX_1	TX_2	Tuner		TX_1	TX_2	Tuner
Width (μm)	Twin Junc.	3.6	7.9	3.6	Single Junc.	3.6	8.7	3.6
Length (μm)		8.5	19.6	7.1		8.0	19.0	7.0

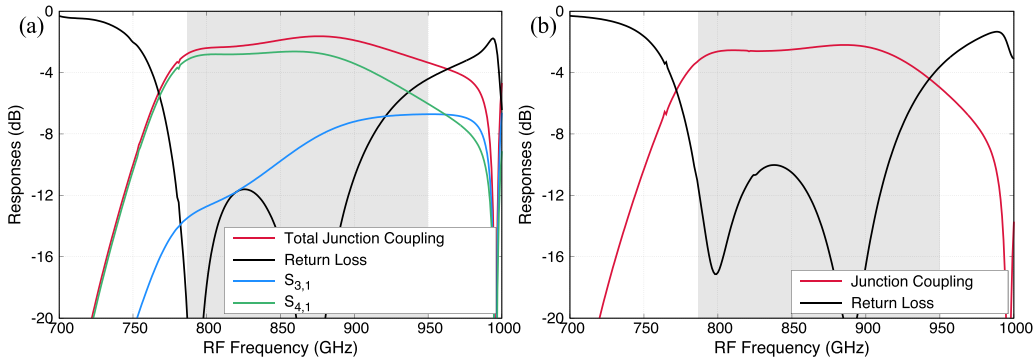

Figure 3. The power coupling from the input rectangular waveguide to the tunnel junction(s) and the return loss performance of the (a) twin-junction tuned and (b) single-junction end-loaded tuned, mixer chips.

3. Heterodyne performance analysis

In this section, we investigate the heterodyning performance of our THz mixers calculated using the SuperMix package [28], developed based on Tucker's quantum theory of mixing. To ensure that we capture the complex and rigorous description of the electromagnetic behaviour of the mixers, we import the scattering matrices generated by the HFSS into SuperMix to form the full circuit model, such that we can produce an accurate prediction of the mixer performance. In particular, we focus on the RF and IF double sideband gain (G_{DSB}) and noise temperature (T_{N}) performance against both designs, as well as the tolerance analysis.

As can be seen from figures 4(a) and (c), we managed to achieve a DSB T_{N} better than twice the quantum limit across the entire RF band from 787–950 GHz, for both designs. The twin-junction model shows a slightly wider RF bandwidth performance, with a better conversion gain overall, compared to the end-loaded design. Rather surprisingly, the effect of an unintended offset of the junction(s) position by $\pm 0.5\,\mu$m with regards to its designated location appears to be not as severe as expected. The behaviour of the twin-junction device is more consistent with the nominal design as this tuning scheme relies only on the relative distance between the two junctions (d_{TJ}), and given that we do not expect that this distance would be different during fabrication, we only simulate the scenarios where both junctions are offset along the same direction with equal displacement. This is justifiable because of the proximity of the junctions and the fact that both junctions would be fabricated using the same mask, hence the major offset will result mainly from the misalignment of the mask against other layers. On the other hand, the effect of the junction offset in the end-loaded design is more pronounced as expected, since the tuning of the junction capacitance relies primarily on the distance between the junction and the edge of TX_2 (d_{EL}). Nevertheless, the error in the junction position seems to only moderately affect the level of conversion gain and shift the bandwidth towards the lower frequency end.

We further investigate the effect of variation in the size of the tunnel junction in figures 4(b) and (d), as this would effectively modify the junction capacitance and normal resistance presented to the mixer circuit, hence affecting the tuning, power coupling and the gain-noise performance. Here we assume the junction area may be varied by $\pm 0.2\,\mu\mathrm{m}^2$, which corresponds to $\pm 40\,\%$ in size, a rather alarming number due to the small nominal junction size of $0.5\,\mu\mathrm{m}^2$ in the designated design. We can see that the gain and noise performance of both mixer designs are certainly affected by the fabrication error at this scale, especially the noticeable shift in the tuning bands. As discussed earlier, the performance of the twin-junction mixer is dominated primarily by the second junction, therefore the variation of the first junction only has a marginal effect. Therefore, the G_{DSB} and T_{N} curves for both designs present largely similar behaviour. In general, the tuning tends to shift toward higher frequency with a slightly broader bandwidth than designated, if the junction turns out to be smaller. However, T_{N} increases from approximately 80 K to about 150 K if the junction is smaller by $0.2\,\mu\mathrm{m}^2$. On the other hand, if the junction area turns out to be larger, interestingly though, T_{N} seems to stay at a similar level as the nominal design, but the bandwidth is comparatively narrower and the performance starts to deteriorate above 0.9 THz.

Figures 4(e) and (f) shows the pumping level for both twin-junction and end-loaded cases, as well as the biasing point used in all the simulations presented here. One noted that the pumping level of the second tunnel junction is much higher than the first junction in the twin-junction design, which is at a similar level as the end-loaded design, again showing the imbalance contribution of the two junctions. However, recall that this plot

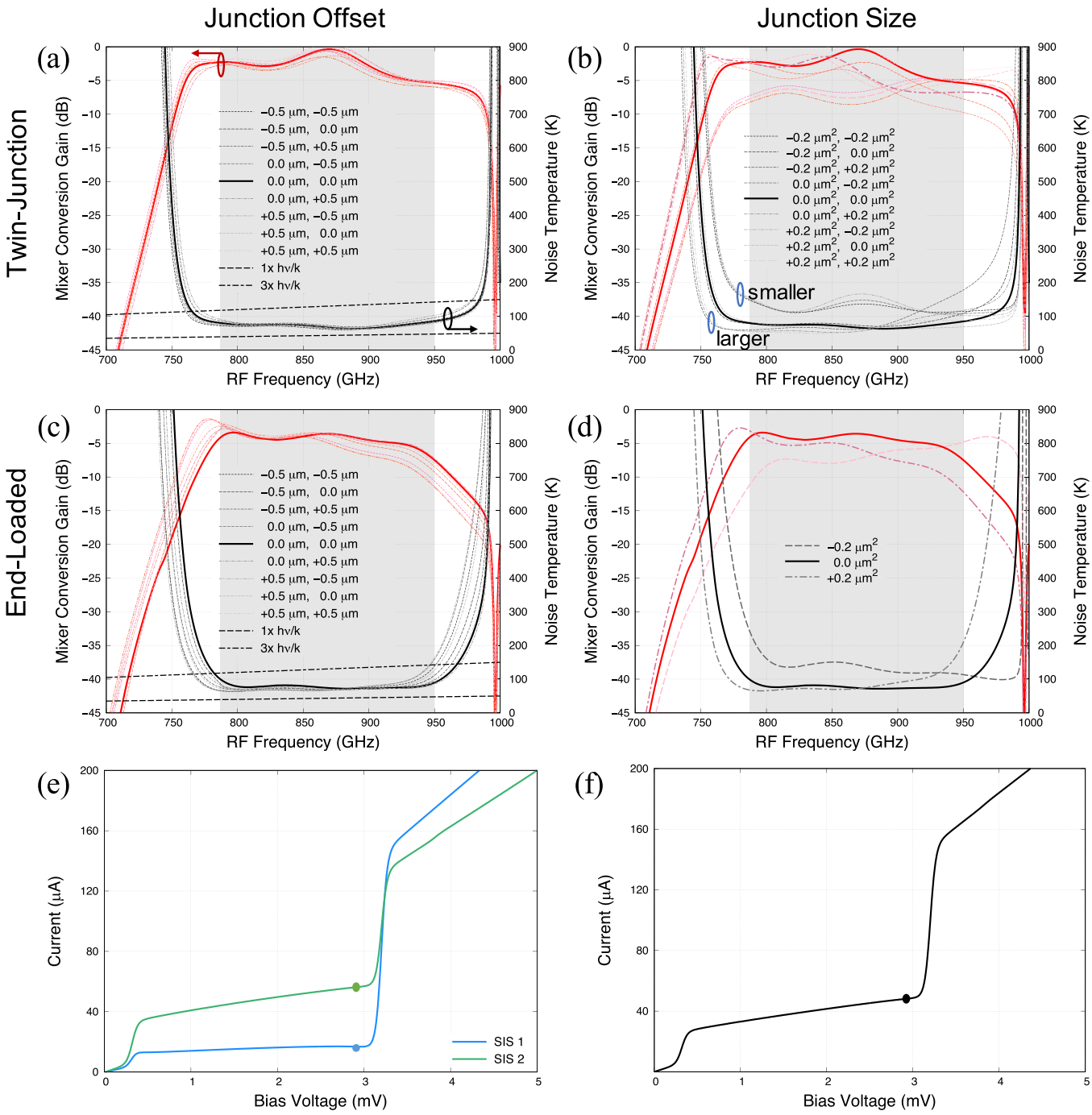

Figure 4. Unless specified, all the fixed parameters for the simulation are set at $f_{RF} = 850$ GHz, $f_{IF} = 0.5$ GHz, $V_{bias} = 2.85$ mV and $Z_{IF} = 50\ \Omega$. The pump levels are adjusted for overall optimal performance across the RF range, hence not reflecting the reality where the pumping level and the bias point are often adjusted at individual RF points during measurement for best performance. Plots (a) and (c) show the predicted G_{DSB} (in various shades of red) and T_N (in various shades of black) across the RF bandwidth for the twin-junction and the end-loaded mixer respectively. The gain and noise temperature deviations are shown for cases where the junction(s) position is offset by $\pm 0.5\ \mu$m. The 1st and 2nd column of the legend in (a) and (c) indicates the offset in the x- (horizontal in figure 1(c)) and y-direction respectively. (b) and (d) Changes in G_{DSB} and T_N caused by variation of $\pm 0.2\ \mu m^2$ in the junction area for twin-junction and end-loaded design respectively. The 1st and 2nd column of the legend in (b) represent the first and second tunnel junction's size. (e) and (f) The pumped IV curves of both mixers, showing the bias point for all simulations.

only shows the junction pumping level near the centre of the band at 850 GHz, and as shown in the power coupling plot of figure 3(a), the pumping level would become closer for both junctions at the higher frequency end.

One important conclusion here is that contrary to the general consensus where twin-junction tuning is believed to be less sensitive to variance in the junction area because the tuning is dominated by the distance between the two junctions,

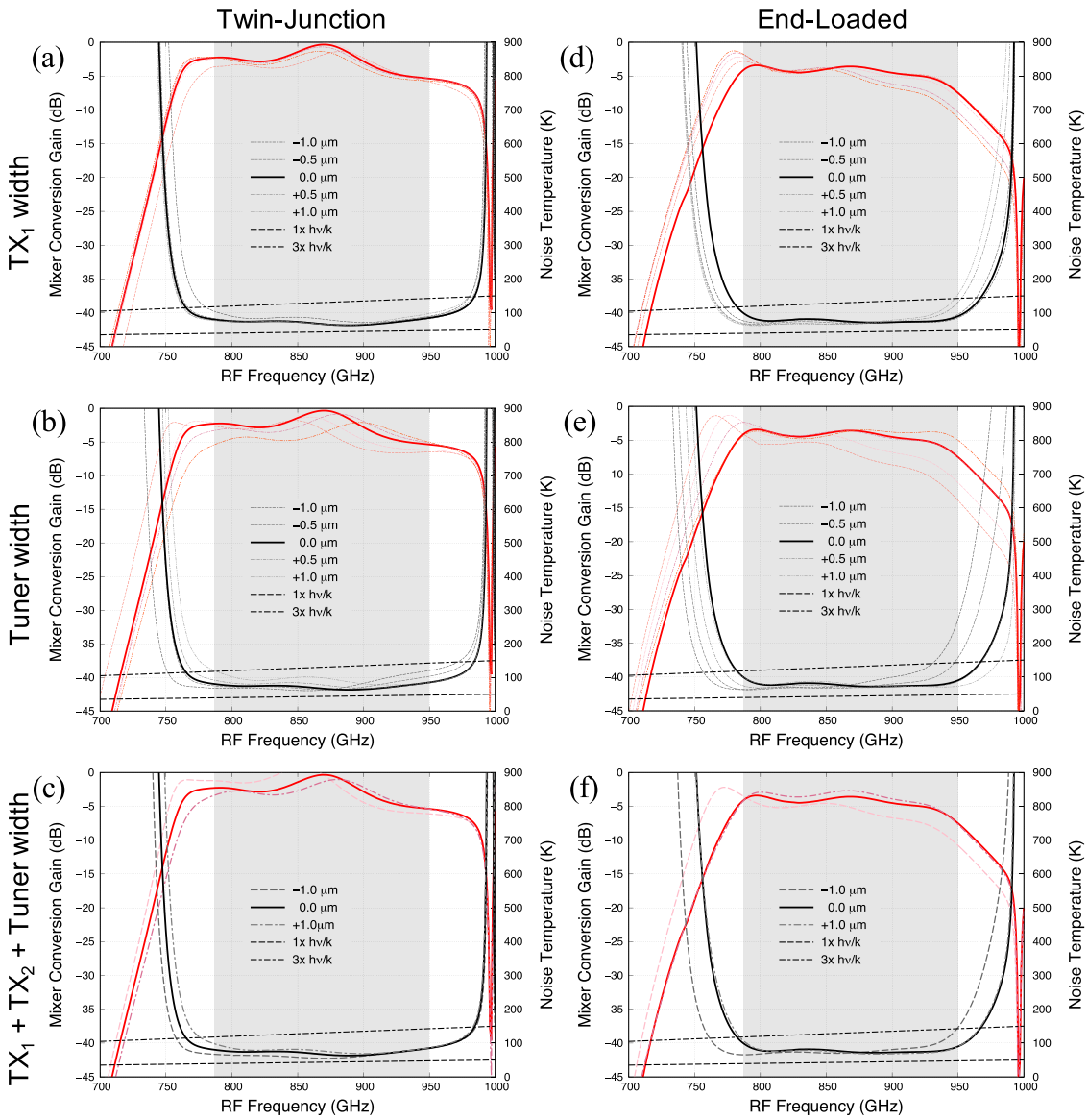

Figure 5. Plots showing how G_{DSB} (in various shades of red) and T_{N} (in various shades of black) responses altered with fabrication errors for cases where: (a) and (d) the width of TX_1 is varied by ± 1 μm; (b) and (e) the width of tuner section is varied by ± 1 μm, (c) and (f) all tuning circuit sections (TX_1, TX_2 and tuner) are varied by ± 1 μm. The left column corresponds to the twin-junction case, while the right column is the end-loaded case.

we found that this is not the case. It is only true if the coupling to both junctions is equal, but in most cases, due to the requirement to achieve broad RF coverage, the junction coupling may not be equal at all range, hence the same affluence to mixer performance at all RF points.

3.1. Tolerance analysis

As explained earlier, various dimensions of the THz circuit components become comparatively smaller, hence the mixer performance would be more susceptible to altercation caused by unexpected errors during the device fabrication process. Hence, in this section, we investigate the scenario where the dimension of several critical circuit components deviates from their optimal value and how this may affect the mixer's performance. Here, we concentrate only on the width of TX_1, TX_2 and the tuner section. We did not include the other dimensions because they are either relatively insensitive to fabrication tolerance due to their larger physical sizes such as the radial probe and the virtual ground patches, or their performance would be indifferent even if their dimension are altered within a reasonable margin such as the RF chokes. We expected that the function of the high impedance line would only be marginally dependent on its width, and is less critical compared to the tuning circuit, hence is opted out from our study here as well.

Comparing the left and right columns of figure 5, which corresponds to the twin-junction and end-loaded design, it is

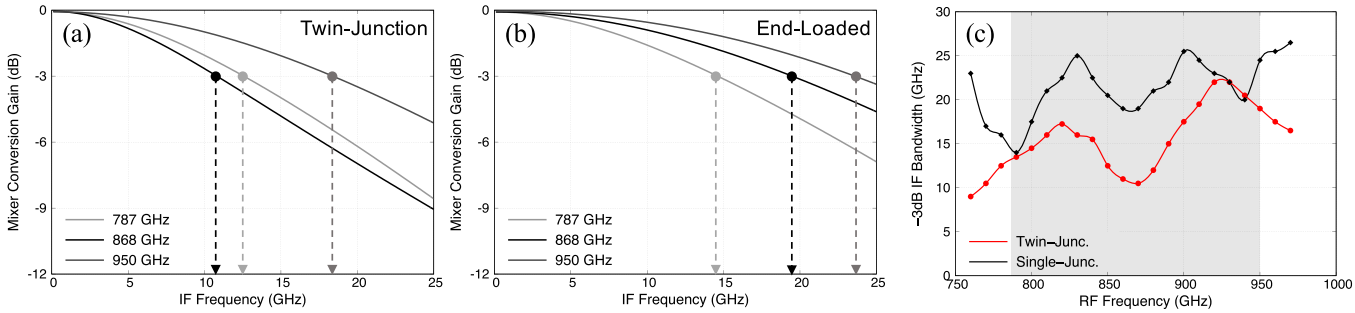

Figure 6. IF gains normalised to the corresponding peak gain predicted by SuperMix at the centre (868 GHz) and the edges of the band (787 and 950 GHz) for (a) the twin-junction, and (b) the end-loaded mixer. The actual peak gain can be inferred from figure 4. All the fixed parameters for these simulations remain the same as that listed in figure 4. (c) IF bandwidth comparison between the two mixer designs across the RF band showing a much superior IF bandwidth performance for the end-loaded design.

rather obvious that overall the former option is slightly more tolerable to the fabrication errors. Relative to the junction offset, the error in the width of TX_1 (Δw_{TX1}) has a less prominent impact for both designs. This is not unanticipated since the function of this section is essentially to provide an intermediate stage to bridge the output impedance of the probe antenna with TX_2, hence a small change in Z_0 would result in almost identical power coupling behaviour, except for a slight shift in the frequency band for the end-loaded design.

Weight against the effect of error in Δw_{TX1}, it is obvious that the change in the width of the tuner section (Δw_{tuner}) for both cases are more prominent, although not alarmingly disastrous. This is because the tuner section is relatively narrow and its characteristic impedance which is controlled by the width is related directly to the junction(s) impedance, hence the coupling. Changes in the width also vary the effective wavelength of the section, hence altering d_{TJ} and d_{EL} in the twin-junction and end-loaded design respectively, practically shifting the tuning away from the central frequency. For the twin-junction case, it tends to displace higher if $\Delta w_{tuner} > 0$, and vice versa, with almost equal magnitude. The same tendency is observed for the end-loaded design, but the frequency swing is asymmetric in this case. It appears that the situation is much worse if $\Delta w_{tuner} < 0$ compared to the scenario when $\Delta w_{tuner} > 0$. Reducing the tuner width by 1 μm could effectively be reducing the bandwidth (especially the upper limit) by close to 50 GHz in this case.

The analyses presented above have provided important insights into the tolerance requirement of each individual section. However, it is more realistic to simulate a scenario where all the tuning circuit widths are altered with the same amount of error margin i.e. either all widths are widened due to over-exposure or turn out to be narrower due to under-exposure, as shown in figures 5(c) and (f). Under these settings, we assume that the junction position(s) remain unchanged to reflect only the effect of a likelier error that may occur during the fabrication process i.e. the deposition of the top wiring layer. Echoing the conclusion reached earlier, we can see that the G_{DSB} and T_N performance of the twin-junction design is less susceptible to fabrication error when all the three sections making up the tuning circuit i.e. Δw_{TX1}, Δw_{TX2} and Δw_{tuner} are varied by ± 1 μm. Generally, narrower widths result in the tuning shifting towards the lower frequency end, and vice versa, by about 10 GHz for the twin-junction model and 20 GHz for the end-loaded design. The simulated behaviour is also largely a resemblance of the effect of Δw_{tuner}, indicating that the tolerance error is dominated by the tuner section since it has the largest impact among the critical dimensions under study. One interesting observation here is that the performance changes for these scenarios seem to be less pronounced than the cases where only Δw_{tuner} is altered. This can be explained by the fact that the change in widths of TX_1 has an opposite effect to the tuner section, where $\Delta w_{TX} < 0$ tend to tune higher, while $\Delta w_{tuner} < 0$ tents to tune lower, hence compensated the overall effect.

This finding is reassuring, as we expect that the changes in Δw would be uniform across all sections. Therefore, we can conclude that both designs are robust against fabrication tolerances as long as the error can be kept within the ± 1 μm margin, which corresponds to ± 30 % changes for Δw_{tuner} and Δw_{TX1}, a rather generous amount. The ± 1 μm error margin is also certainly within the limit of modern photolithography fabrication technique, hence we are confident that our mixers will yield measured results that match the predicted performance.

3.2. IF performance comparison

Finally, we investigate the IF bandwidth performance for both THz mixers. Here, we used the –3 dB level of the IF conversion gain (G_{IF}) as an indicator for the bandwidth limit. It is worthwhile noting that the IF conversion gain curve's flatness and the bandwidth limit can be improved by using an intermediate stage IF transformer to bridge the impedance mismatch between the mixer output impedance with the 50 Ω IF chain [26, 29], but due to the layout of the existing THz mixer block, at present, there is no provision for accommodating additional IF components.

Figures 6(a) and (b) shows the IF conversion gain curves normalised to the peak gain near the edges as well as at the centre of the band, for the twin-junction and end-loaded design respectively. Comparing the two, it is clear that the rate of deterioration towards the higher microwave frequency range is

more rapid in the twin-junction case. This rate of gain deterioration is dependent on the RF frequency as it is related to the maximum RF gain at that particular RF point, and it generally rolls off faster when the peak gain is higher. Furthermore, one noted immediately that at all three RF points, the –3 dB bandwidth of the end-loaded mixer is far superior to the twin-junction design, offering an IF bandwidth as broad as 24 GHz.

The same analysis is presented in figure 6(c), where we now plot the –3 dB IF bandwidth across the entire RF band. As shown in the figure, in all cases, we can achieve better than 10 GHz bandwidth. However, it is obvious that the end-loaded design offers a much better IF bandwidth performance, wider than 20 GHz for most of the RF range, except below 800 GHz. Comparatively, the IF bandwidth of the twin-junction mixer is almost always half of that of the end-loaded case. Therefore, we argue that given the RF performance of both designs are largely similar, and as long as we can minimise the fabrication error, this huge advantage of doubling the IF bandwidth performance using the end-loaded design with only one tunnel junction employed would offer a much better overall performance merits.

4. Conclusion

We have described the designs of two THz mixers centred near 850 GHz, utilising either two parallel junctions or an end-loaded tuning scheme with only one junction employed. We presented a comprehensive analysis of the mixer behaviour, including various extensive studies on the fabrication tolerances and how they may affect the mixer performance, and the findings are encouraging. We, therefore, concluded that our mixer designs are relatively robust against fabrication error as long as the various features can be contained within the ± 1 μm error margin and the junction position can be kept within the ± 0.5 μm limit. Furthermore, we found that as long as the junction area variation can be kept at a level less than ± 40 %, the mixer would still operate well across most parts of the RF coverage range.

Although the twin-junction design is better in terms of resilience to fabrication error and presented slightly wider RF bandwidth performance, these advantages are of little account compared to the much superior IF bandwidth performance from the end-loaded design. Indeed, with the current design, we successfully cover the entire required RF range from 787 to 950 GHz, but the IF bandwidth is now improved significantly, almost double that of the twin-junction design. This is important given the recent requirement of various mm/sub-mm instruments, such as ALMA observatory that prefer ultra-wide IF bandwidth to reduce the need to retune the local oscillator frequently and therefore allow faster observation speed with better spectrum coverage that may capture several spectral lines simultaneously. Hence, we conclude that the end-loaded design with a single junction is a better solution at the THz regime because it has a much better intrinsic heterodyning performance. Therefore, the effort should now be concentrated on minimising the fabrication error so that the fabricated mixers would achieve the expected RF and IF performance.

Data availability statement

All data that support the findings of this study are included within the article (and any supplementary files).

Acknowledgments

This research was funded in part by the European Union's Horizon 2020 research and innovation programme under Grant Agreement No 730562 (RadioNet), the Russian Foundation for Basic Research (No 19-52-80023) and the UK-STFC Consortium Grant (ST/R00062X/1). For the purpose of Open Access, the author has applied a CC BY public copyright licence to any Author Accepted Manuscript version arising from this submission.

Appendix. Improving the RF performance of the single-junction mixer

As shown in the main text, our end-loaded mixer has a much better IF bandwidth performance, but the RF bandwidth is slightly narrower than the twin-junction design, even though in our case, it is sufficient to cover the entire RF range required. As hinted earlier, there exists another variation of the single-junction tuning scheme, utilising a short microstrip section i.e. a stub, connected after the tunnel junction to tune out the capacitance, instead of before the junction. The stub practically transforms either a 'short-circuit' or an 'open-circuit' end over a certain length to present an equivalent inductive value to the junction, hence cancelling out the junction capacitance over a certain frequency range. Therefore, to broader the bandwidth of the end-loaded design, although not expected to be dramatically improved, we can indeed incorporate an additional stub after the end-loaded tuner to better the RF bandwidth [17, 30] while retaining the advantage at the IF range with only a single-tunnel junction. Since this improved bandwidth design only adds a short microstrip section after the junction, we do not expect the tolerance analysis for this design to be immensely different from the analysis presented earlier.

Figure A1(a) shows the layout of the new tuner design, which is almost identical to the end-loaded mixer except for the additional short stub added after the tunnel junction. The additional end-stub was added to retune the mixer circuit moderately at a slightly different frequency to complement that of the end-loaded tuner. All sections comprising the tuner circuit i.e. TX_1, TX_2, the tuner section and the end-stub are re-optimised for optimal power coupling using HFSS. The optimised dimensions of all sections are listed in table A1. As shown in figure A1(b), with such modification,

Table A1. Dimensions of the various sections forming the end-loaded with an additional end-stub tuning circuit.

	TX_1	TX_2	Tuner	End-Stub
Width (μm)	3.6	8.7	3.6	3.0
Length (μm)	8.0	19.0	7.0	2.5

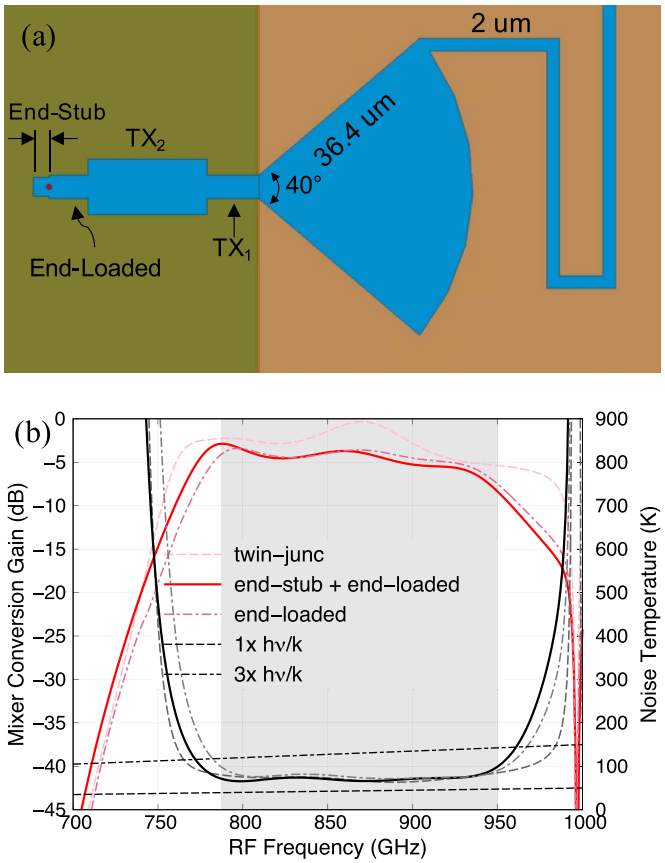

Figure A1. (a) Detail of the radial probe and the end-loaded with an additional end-stub tuning circuit, which is largely similar to the original end-loaded design, apart from the additional short microstrip stub after the junction. (b) DSB gain and noise temperature performance comparison between the new tuning methods and the original two presented in the main text.

we successfully broaden the RF bandwidth of the original single-junction mixer design by approximately 15 GHz. The DSB gain of the new design is also improved by more than 2 dB with a better noise temperature of about 20 K below 850 GHz. As the tuner dimensions are largely similar to the end-loaded design, with only a minor addition of the end-stub section, we do not expect that the tolerance analysis and the IF bandwidth performance would be vastly dissimilar, hence a slightly better-performing single-junction THz mixer design.

ORCID iDs

B-K Tan https://orcid.org/0000-0002-6252-9351
V P Koshelets https://orcid.org/0000-0002-1563-1257

References

[1] Combes Fçoise *et al* 2000 *Molecular Hydrogen in Space* (Cambridge: Cambridge University Press)
[2] Herbst E and Van Dishoeck E F 2009 Complex organic interstellar molecules *Annu. Rev. Astron. Astrophys.* **47** 427–80
[3] Caselli P 2011 Observational studies of pre-stellar cores and infrared dark clouds *Proc. Int. Astron. Union* vol 7 pp 19–32
[4] Rigopoulou D, Laing R, Withington S, Magdis G, Graves S, Richer J and Ellison B 2013 Science with ALMA band 11 (1.0–1.6 THz) *Messenger* **153** 35–37
[5] Uzawa Y *et al* 2015 Tuning circuit material for mass-produced terahertz SIS receivers *IEEE Trans. Appl. Supercond.* **25** 1–5
[6] De Lange G, Jackson B D, Jochemsen M, Laauwen W M, De Jong L, Kroug M, Zijlstra T and Klapwijk T M 2006 Performance of the flight model HIFI band 3 and 4 mixer units *Proc. SPIE* **6275** 627517
[7] Khudchenko A, Baryshev A M, Rudakov K I, Dmitriev P M, Hesper R, Leo de J and Koshelets V P 2016 High-gap Nb-AlN-NbN SIS junctions for frequency band 790–950 GHz *IEEE Trans. Terahertz Sci. Technol.* **6** 127–32
[8] Khudchenko A *et al* 2017 Performance of SIS mixers for upgrade of CHAMP+ 7-pixel arrays *Proc. 28th Int. Symp. on Space Terahertz Technology*
[9] Jackson B D, Gert de L, Zijlstra T, Kroug M, Kooi J W, Stern J A and Klapwijk T M 2006 Low-noise 0.8-0.96-and 0.96-1.12-THz superconductor-insulator-superconductor mixers for the Herschel space observatory *IEEE Trans. Microw. Theory Tech.* **54** 547–58
[10] Kojima T, Kroug M, Takeda M, Uzawa Y, Shan W, Fujii Y, Wang Z and Ogawa H 2009 Three quanta sensitivity superconductor–insulator–superconductor mixer for the 0.78–0.95 THz band *Appl. Phys. Express* **2** 102201
[11] Uzawa Y, Kroug M, Kojima T, Makise K, Gonzalez A, Saito S, Fujii Y, Kaneko K, Terai H and Wang Z 2016 Design of terahertz SIS mixers using Nb/AlN/Nb junctions integrated with all-NbTiN tuning circuits *IEEE Trans. Appl. Supercond.* **27** 1–5
[12] Karpov A, Miller D, Rice F, Stern J A, Bumble B, LeDuc H G and Zmuidzinas J 2007 Low Noise 1 THz–1.4 THz mixers using Nb/Al-AlN/NbTiN SIS junctions *IEEE Trans. Appl. Supercond.* **17** 343–6
[13] Yassin G, Baryshev A M and Honigh N 2019 Reports on the development of SIS tunnel junctions and SIS mixers at 1.0 THz (available at: https://ec.europa.eu/research/participants/documents/downloadPublic?documentIds=080166e5c9f24aad&appId=PPGMS)
[14] Traini A, Tan B-K, Garrett J D, Khudchenko A, Hesper R, Baryshev A M, Dmitriev P N, Koshelets V P and Yassin G 2020 The influence of LO power heating of the tunnel junction on the performance of THz SIS mixers *IEEE Trans. Terahertz Sci. Technol.* **10** 721–30
[15] Tan B-K, Mahashabde S, Hector A, Yassin G, Khudchenko A, Hesper R, Baryshev A M, Dmitriev P, Rudakov K and Koshelets V P 2018 Investigation of the performance of an SIS mixer with Nb-AlN-NbN tunnel junctions in the 780–950 GHz frequency band *Proc. 29th Int. Symp. on Space Terahertz Technology* (National Radio Astronomy Observatory)
[16] Risacher C, Vassilev V, Pavolotsky A and Belitsky V 2003 Waveguide-to-microstrip transition with integrated bias-T *IEEE Microw. Wirel. Compon. Lett.* **13** 262–4
[17] Tan B K 2015 *Development of Coherent Detector Technologies for sub-Millimetre Wave Astronomy Observations* (Berlin: Springer)

[18] Origin Space Telescope (OST) (available at: https://asd.gsfc.nasa.gov/firs/)
[19] Rigopoulou D *et al* 2021 The far-infrared spectroscopic surveyor (FIRSS) *Exp. Astron.* **51** 1–30
[20] Parshley S C *et al* 2018 CCAT-prime: a novel telescope for sub-millimeter astronomy *Proc. SPIE* **10700** 107005X
[21] Smirnov A *et al* 2020 Development status of the millimetron space observatory *Space Telescopes and Instrumentation 2020: Optical, Infrared and Millimeter Wave* vol 11443 (International Society for Optics and Photonics) p 114432H
[22] Baryshev A M *et al* 2015 The ALMA Band 9 receiver—design, construction, characterization and first light *Astron. Astrophys.* **577** A129
[23] Belitsky V Y and Tarasov M A 1991 SIS junction reactance complete compensation *IEEE Trans. Magn.* **27** 2638–41
[24] Zmuidzinas J, LeDuc H G, Stern J A and Cypher S R 1994 Two-junction tuning circuits for submillimeter SIS mixers *IEEE Trans. Microw. Theory Tech.* **42** 698–706
[25] Belitsky V Y, Jacobsson S W, Filippenko L V and Kollberg E L 1995 Broadband twin-junction tuning circuit for submillimeter SIS mixers *Microw. Opt. Technol. Lett.* **10** 74–78
[26] Tan B-K, Yassin G and Grimes P 2014 Ultra-wide intermediate bandwidth for high-frequency SIS mixers *IEEE Trans. Terahertz Sci. Technol.* **4** 165–70
[27] Kooi J W 2008 *Advanced Receivers for Submillimeter and Far Infrared Astronomy* (Rijkuniversiteit Groningen)
[28] Ward J, Rice F, Chattopadhyay G and Zmuidzinas J 1999 SuperMix: a flexible software library for high-frequency circuit simulation, including SIS mixers and superconducting elements *Proc. 10th Int. Symp. on Space Terahertz Technology* pp 269–81
[29] Tan B-K, Yassin G and Grimes P 2013 A simple method to widen the IF bandwidth of a high frequency SIS mixer *Proc. 24th Int. Symp. on Space Terahertz Technology* (National Radio Astronomy Observatory)
[30] Tan B-K, Yassin G, Grimes P, Leech J, Jacobs K and Groppi C 2011 A 650 GHz unilateral finline SIS mixer fed by a multiple flare-angle smooth-walled horn *IEEE Trans. Terahertz Sci. Technol.* **2** 40–49